## Original Article

# Curculigoside alleviates ferroptosis in renal interstitial fibrosis by regulating the Nrf2/HO-1 signaling pathway

Tianyuan Liu<sup>1</sup>, Manshu Sui<sup>1</sup>, Chengyuan Yu<sup>2</sup>, Yushi Bao<sup>1</sup>, Li Xing<sup>1</sup>, Donghua Hou<sup>3</sup>, Rujuan Xie<sup>1</sup>

<sup>1</sup>Department of Nephrology, The First Affiliated Hospital of Harbin Medical University, Harbin 150000, Heilongjiang, China; <sup>2</sup>Department of Gerontology, Shenzhen People's Hospital, Shenzhen 518020, Guangdong, China; <sup>3</sup>Department of Hemodialysis, The First Affiliated Hospital of Harbin Medical University, Harbin 150000, Heilongjiang, China

Received March 31, 2025; Accepted September 15, 2025; Epub October 15, 2025; Published October 30, 2025

Abstract: Objectives: Renal interstitial fibrosis (RIF) represents the final pathway in most progressive renal diseases. Curculigoside (CCG), derived from Curculigo Pilosa, affects oxidative stress and inflammation. However, the effects of CCG on RIF remain unclear. This study explored the nephroprotective role of CCG in regulating oxidative stress through the nuclear factor erythroid 2-related factor 2 (Nrf2)/heme oxygenase-1 (HO-1) pathway. Methods: Bioinformatic analysis was employed to identify the targets of CCG, elucidate the underlying pathways, and analyze molecular docking results. C57BL/6 mouse models of unilateral ureteral obstruction (UUO) were established to validate the results. Morphologic changes were assessed by pathologic examination, and the expression of proteins associated with renal ferroptosis and fibrosis was analyzed by western blotting. Additionally, the levels of glutathione (GSH), malondialdehyde (MDA), superoxide dismutase (SOD), and iron were measured. Results: In total, 3,532 differentially expressed genes (DEGs) were identified, comprising 2,290 upregulated and 1,242 downregulated genes. We retrieved 484 ferroptosis-related genes from the ferroptosis regulators (FerrDb) database, identifying 143 DEGs after intersecting with those from the Gene Expression Omnibus Series 217654 dataset (GSE217654). The key identified genes included nicotinamide adenine dinucleotide oxidase 4 (NOX4), activating transcription factor 3 (ATF3), mitogen-activated protein kinase 14 (MAPK14), tissue inhibitor metalloproteinase 1 (TIMP1), and early growth response 1 (EGR1). Gene Ontology (GO) and Kyoto Encyclopedia of Genes and Genomes (KEGG) analyses indicated that these genes were enriched in oxidative signaling pathways. The results exhibited the docking activity of CCG with related targets. CCG significantly alleviated histopathologic damage, reduced MDA and iron levels, and increased GSH and SOD levels. Protein analysis indicated that CCG alleviated fibrosis and enhanced the protein expression of antioxidants in UUO kidney tissues. CCG activated the Nrf2/HO-1 pathway and reduced UUO-induced ferroptosis. Conclusions: CCG may improve renal fibrosis and mitigate ferroptosis by activating the Nrf2/HO-1 signaling pathway.

Keywords: Renal interstitial fibrosis, curculigoside, ferroptosis, UUO, bioinformatics

## Introduction

Chronic kidney disease (CKD) constitutes a growing global public health challenge, characterized by an increasing incidence [1]. Renal interstitial fibrosis (RIF) is characterized by excessive deposition of extracellular matrix (ECM) in the renal interstitium [2]. RIF commonly affects glomerular podocytes, which are critical for remodeling the glomerular basement membrane (GBM) and forming filtration slits between the interdigitating foot processes [3]. These changes result in podocyte detachment from the GBM, damage to the fissure mem-

brane, increased protein filtration, and kidney shrinkage [4]. However, there is no specific treatment for renal interstitial fibrosis in CKD, and dialysis has limitations in addressing fibrosis-related renal damage [5, 6]. Therefore, the molecular regulatory mechanisms underlying renal fibrosis should be explored, and suitable treatments should be investigated [7].

Studies have identified a correlation between ferroptosis and renal interstitial fibrosis; however, the exact role of ferroptosis in this context remains unclear [8]. Ferroptosis is an iron-dependent mechanism characterized by thicker

lipid bilayer membranes and reduced cell connectivity, leading to cell detachment [9]. Ferroptosis involves complex regulatory mechanisms, including antioxidants, lipids, and iron metabolism pathways [10]. Glutathione (GSH) and glutathione peroxidase 4 (GPX4) are crucial for lipid repair, exhibiting strong antioxidant properties [11]. In case of GPX4 insufficiency, superoxide accumulation leads to ferroptosis [12]. To date, no chemical or natural drugs have shown a definitive effect on renal fibrosis; therefore, it is necessary to explore alternative treatments.

Active ingredients in traditional Chinese medicine (TCM) are commonly used to treat diseases [13]. CCG, a traditional Chinese medicinal plant, has demonstrated anti-inflammatory and antioxidant properties in various diseases, including osteoporosis, idiopathic pulmonary fibrosis, and ulcerative colitis [14-16]. Despite numerous studies demonstrating the pharmacologic benefits of CCG in combating oxidative stress, studies regarding its efficacy in treating CKD remain inconclusive. Due to its extensive computational capabilities, bioinformatics has recently enabled the analysis of disease mechanisms from various aspects [17]. It challenges the traditional paradigm of "one disease-one target-one drug", elucidates the mechanisms underlying complex diseases, and can be effectively employed in conjunction with molecular docking techniques [18]. Therefore, identifying natural products based on bioinformatics and molecular docking provides novel insight into drug development.

Nrf2, a redox-sensitive transcription factor, protects against oxidative damage [19]. The Nrf2/ARE signaling pathway significantly enhances the expression of the downstream protein HO-1 [20]. Evidence suggests that HO-1 is a pivotal protein for ferroptosis [21]. However, the potential relationship between CCG, Nrf2/HO-1, and RIF warrants further investigation.

In this study, C57BL6 mice were chosen to establish *in vivo* models of UUO, with CCG as the intervention. The results demonstrated that CCG improved renal interstitial fibrosis by mitigating oxidative stress. Bioinformatics and molecular docking indicated that CCG acted through the Nrf2/HO-1 signaling pathway. These results suggest that CCG significantly protects against renal fibrosis, offering a valu-

able foundation for further clinical research on the treatment of CKD.

## Materials and methods

Targeted genes, data processing, and data sources

The gene expression profile of renal interstitial fibrosis was obtained from the GEO database (https://www.ncbi.nlm.nih.gov/geo/) with GSE number GSE217654. After log transformation and normalization, a differential analysis was conducted using the limma package of R. Gene annotation information from GPL28457 was used to convert probe IDs to gene symbols. Data on ferroptosis-related genes, encompassing drivers, markers, and suppressor genes, were obtained from the FerrDb database (http://www.zhounan.org/ferrdb/legacy/). Volcano plots and heatmaps were created utilizing the ggplot2 and heatmap packages, respectively. Venn diagrams were constructed using the Venn Diagram package. All analyses were conducted using R software (version 4.4.4). The Random Forest SRC package of R was used for machine learning to screen genes and identify the most predictive combination of ferroptosis-fibrosis markers. After z-score normalization of gene expression data, they were visualized using PheatMap.

## Bioconcentration analysis

Biological enrichment analysis is crucial to understanding how CCG affects renal interstitial fibrosis. This included Gene Ontology (GO) functional enrichment and Kyoto Encyclopedia of Genes and Genomes (KEGG) pathway enrichment using the clusterProfiler package of R. Correlations between genes linked to ferroptosis and differentially expressed genes (DEGs) were analyzed using the STRING database. The ClusterProfiler package was used for KEGG mapper enrichment analysis. Ggplot2 was used for data visualization to reveal the key pathway intersections of those five genes. Results with *p*-values of less than 0.05 were visualized using the ggplot2 package.

## Molecular docking

The keyword "curculigoside" was used to retrieve its small molecular structure file from the PubChem database. Three-dimensional

structures of Acyl-COA synthetase long-chain family member 4 (ACSL4), GPX4, and solute carrier family 7 member 11 (SLC7A11/xCT) were obtained from the Protein Data Bank (PDB). The protein files underwent preprocessing utilizing Python Molecular Viewer (PyMOL) software. Flexible docking was employed to account for the side-chain flexibility of key residues in the binding pocket. During the docking process, rotatable bonds were allowed for both the ligand and the receptor. Docking calculations and validations involving the small molecule CCG and proteins were conducted using Autodock 1.5.7 software, resulting in multiple docking outcomes that were subsequently viewed and analyzed using PyMOL.

## Reagents

As a lyophilized product, CCG (HY-N0705) was provided by MCE (China). ML385 (HY-100523) and ferrostatin-1 (HY-100579) were purchased from MCE (China), and transforming growth factor- $\beta$ 1 (TGF- $\beta$ 1) (10804-HNAC) was purchased from Sino Biological (China). Fetal bovine serum (FBS, PB180438) was purchased from Pricella (China). SOD (A001-1-2), GSH (A006-1-1), MDA (A003-1-2), and iron assays (A039-2-1) were purchased from Jiancheng Bioengineering Institute (China).

#### Animals

Animal experiments were conducted after obtaining the approval of the Ethics Committee at the First Affiliated Hospital of Harbin Medical University, China (Approval No. 2023069). Forty-eight male C57BL/6 mice, aged 8 weeks and weighing no more than 20 g (Liaoning Changsheng Company, China), were housed indoors, with a controlled 24-hour light cycle, and continuous access to a standard diet and fresh water.

## Experimental protocol

Forty-eight mice were randomly allocated to eight distinct groups: Sham, UUO, UUO+ 1.25 mg/kg CCG; UUO+ 2.5 mg/kg CCG; UUO+ 5 mg/kg CCG; UUO+ 30 mg/kg ML385 (Nrf2 inhibitor); UUO+ 5 mg/kg CCG+ 30 mg/kg ML385; UUO+ 5 mg/kg Fer-1 (ferrostatin-1). Mice were anesthetized with 1% amobarbital sodium and then subjected to UUO by ligating the left ureter. All treatment groups received

drugs three hours before modeling by gavage, while ML385 and Fer-1 were administered intraperitoneally. CCG and Fer-1 were administered for 2 weeks, while treatment with ML385 was continued for 1 week. The mice were euthanized after the intervention. The renal tissues were isolated and weighed. A portion of the kidney tissue was fixed in 10% formalin for histopathologic and immunohistochemical staining, while the remaining tissues were frozen at -80°C for further analysis.

## Histopathologic analysis

The kidney tissues were examined by staining 3-µm slices with Masson's trichrome and hematoxylin-eosin (H&E). After deparaffinizing and hydrating, the slides were rinsed with distilled water. Subsequently, the cells were exposed to 3% hydrogen peroxide at room temperature for 10 min. Subsequently, they were incubated in 10% goat serum for 30 min. The slides were then incubated overnight at 4°C with antibodies against the following proteins: GPX4 (1:100, CY6959, Abways), ACSL4 (1:500, 66617-1-Ig, Proteintech), Nrf2 (1:100, CY5136, Abways), and recombinant solute carrier family 7/member 11 (SLC7A11/xCT) (1:100, Affinity). Next, following the initial incubation, the samples were incubated with a secondary antibody conjugated with peroxidase (RS0002, diluted 1:100, Immunoway) for one hour. After 30 minutes of diaminobenzidine (DAB) development and counterstaining with hematoxylin, the tissues stained immunohistochemically were ready for further processing. The sections were analyzed using a digital slide scanner (3DHistech Ltd.), and ImageJ software was used to quantify the positive staining areas.

## Western blotting

Kidney tissue proteins were extracted using a radioimmunoprecipitation assay buffer (RIPA) kit (Beyotime, China). Protein samples (40 μg) were separated on 7.5% and 10% SDS-PAGE gels, and then transferred to polyvinylidene fluoride (PVDF) membranes (Roche, USA). After a 1.5-hour incubation at room temperature, the membranes were blocked with 5% non-fat milk. Primary antibodies against β-actin (YM8010, 1:1000, Immunoway), Nrf2 (16396-1-AP, 1:5000, Proteintech), xCT (CY7046, 1:1000, Abways), GPX4 (CY6959, 1:500, Abways), ACSL4 (66617-1-Ig, 1:3000, Abways),

HO-1 (10701-1-AP, 1:3000, Proteintech), collagen type I (66761-1-Ig, 1:2000, Proteintech), and fibronectin (66042-1-Ig, 1:2000, Proteintech) were then applied. Subsequently, the PVDF membranes were incubated with peroxidase-conjugated secondary antibodies (RS23-910, RS23920, Immunoway) for one hour at ambient temperature. ImageJ software was used to quantify band intensity.

Measurement of SOD, GSH, and MDA levels and iron analysis

The hydroxylamine technique was used to determine superoxide dismutase (SOD) levels. A spectrophotometric method was employed to determine GSH concentrations. The thiobarbituric acid method was employed to measure MDA levels. A standard curve was used to determine the level of oxidative stress and protein content in each sample. Renal tissues from each group were cut into 10-milligram pieces, rinsed with ice-cold phosphate-buffered saline (PBS), and homogenized using the A039-2-1 iron assay kit (Jiancheng Bioengineering Institute, China) to measure iron levels in kidney tissues.

#### Statistical analysis

Statistical analyses were conducted using GraphPad Prism version 10.0. Data were presented as mean ± standard deviation (SD). One-way analysis of variance (ANOVA) followed by Tukey's post hoc test was employed for comparisons. The T-test was used for analyzing boxplots. The correlation between genes was calculated using Spearman correlation analysis to form Co-expression heatmaps. A *P*-value of less than 0.05 was considered significant.

### Results

Ferroptosis-related DEGs and PPI network analysis of ferroptosis-related DEGs

GSE217654 was obtained from the GEO query to obtain the expression profile data related to RIF. The dataset GSE217654 comprised three UUO samples and five control samples obtained by integrating two distinct transcriptional data profiles. In total, 3,532 DEGs related to tubulointerstitial lesions were identified, and 484 ferroptosis-related genes were obtained from the FerrDb database. We identified 143 ferrop-

tosis-related DEGs by intersecting these DEGs with those from GSE217654 (Figure 1A). There were 2,290 upregulated and 1,242 downregulated genes (Figure 1B and 1C). The 143 ferroptosis-related DEGs are presented in a Venn diagram and table (Figure 1D; Table 1). By integrating the results from CytoHubba algorithms, we identified five key genes, including NOX4, ATF3. MAPK14. TIMP1. and EGR1 (Figure 1E: Table 2). Notably, five hub genes, including MAPK14, ATF3, NOX4, TIMP1, and EGR1, were annotated as ferroptosis drivers (Table 1). MAPK14 and NOX4 were upregulated in the control group, while downregulated in the UUO group; the expression of ATF3, TIMP1, and EGR1 showed an opposite pattern (Figure 2).

Bioinformatic analysis of core ferroptosis regulators in RIF

To delineate the pro-ferroptotic or anti-ferroptotic roles of the identified genes, we analyzed their classification using FerrDb. NOX4 is highly expressed in the kidney [22, 23]. NOX4 has been suggested to contribute to renal fibrosis in ischemia/reperfusion-induced acute kidney injury (AKI) [8]. NOX4 was downregulated in the UUO group in the GSE217654 dataset (P<0.001). Pearson analysis indicated that it was negatively correlated with GPX4 (P<0.05). xCT (P<0.05) and ACSL4 (P<0.01) (Figure 3A, 3G). ATF3 was initially identified both before and after renal ischemia and reperfusion [24]. Additionally, ATF3 upregulation was found to exacerbate ferroptosis [25]. ATF3 was upregulated in the UUO group of the GSE217654 dataset compared to the control group (P<0.001). It was not statistically correlated with GPX4 (P>0.05) but was negatively correlated with xCT (P<0.01) and ACSL4 (P<0.01) (Figure 3B, 3G). MAPK14 plays a critical role in DNA damage and repair [26], is involved in cellular growth and apoptosis [27], and is enriched in 58 pathways in the pathogenesis of AKI-diabetes comorbidity [28]. In the UUO group, MAPK14 was downregulated (P<0.001), and negatively correlated with GPX4 (P<0.01), xCT (P<0.01), and ACSL4 (P<0.01) (Figure 3C, 3G). TIMP1 was upregulated in the UUO group (P<0.001), consistent with the findings in a rat model of Ischemia-Reperfusion injury (IRI) renal tissue [29]. It was negatively correlated with GPX4 (P<0.01), xCT (P<0.05), and ACSL4 (P<0.01) (Figure 3D, 3G). EGR1 was upregulated in the

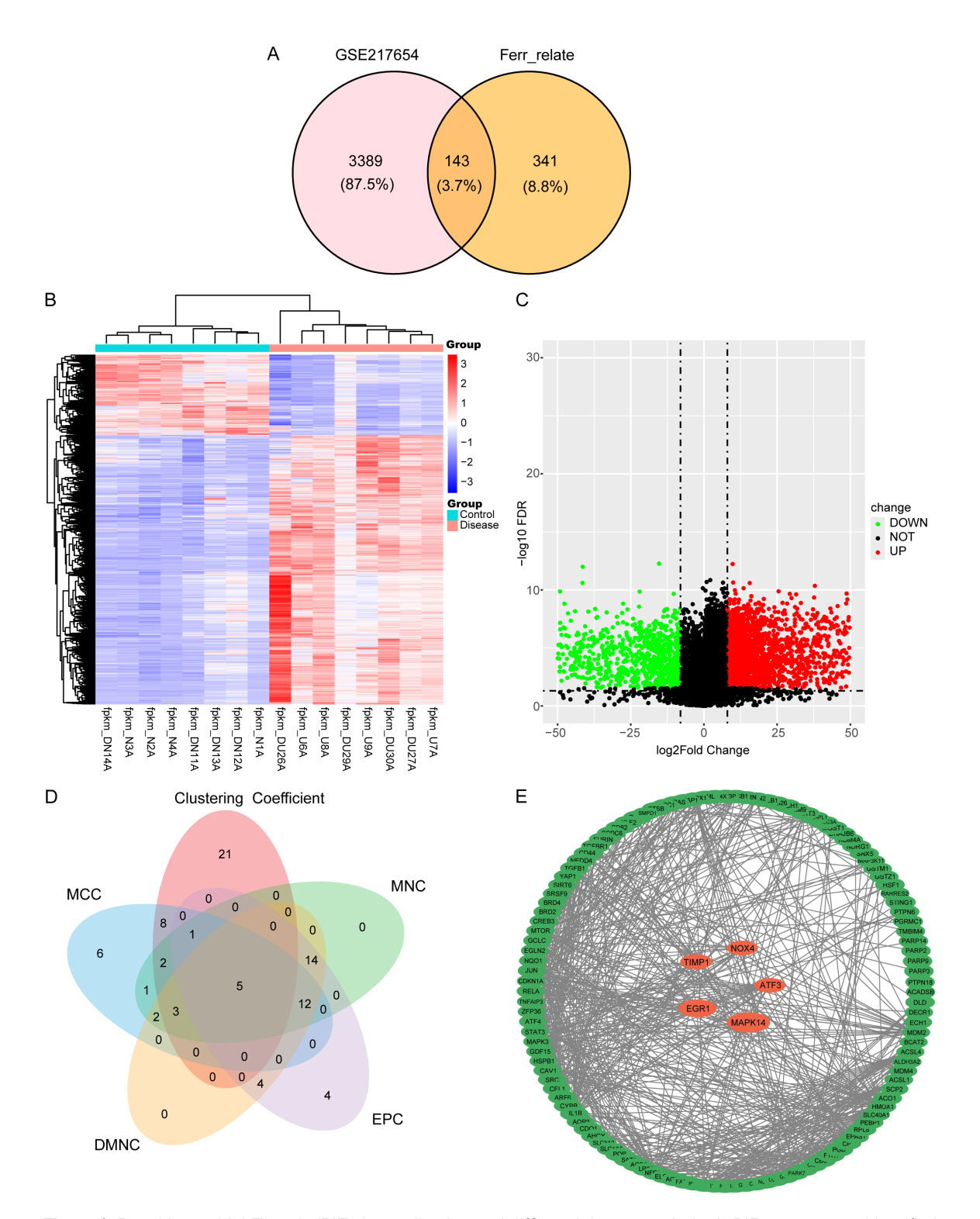


Figure 1. Renal Interstitial Fibrosis (RIF) data collection and differential gene analysis. A. RIF target genes identified from the Gene Expression Omnibus (GEO) differential gene analysis and the ferroptosis target database. B. A heatmap of 3,532 Differentially Expressed Genes (DEGs), with expression levels color-coded: red for high expression and blue for low expression. C. Volcano plots depict DEGs between sham and unilateral ureteral obstruction (UUO) groups, applying the criteria of |log2 (fold change)| >1 and P. adjust <0.05. Red points represent 2,290 up-regulated genes. Black points indicate 15,626 non-significant differences, and green points denote 1,242 down-regulated genes. D. A Venn diagram showcasing five key genes identified through the intersection of the results from five CytoHubba algorithms. E. The protein interaction network illustrates interactions among proteins or genes related to RIF associated with ferroptosis, comprising 133 nodes and 51 edges for ferroptosis-related DEGs in this context.

**Table 1.** Ferroptosis-related differentially expressed genes (DEGs), including ferroptosis drivers, suppressors, and markers

Driver	Marker	Suppressor
STING1, AGPS, OSBPL9	HSPB1, SLC40A1 NFE2L2, FTH1, GPX4	AHCY, MTOR, CP
GSTZ1, NRAS, SIRT3, MAPK3		RELA, SRC, STAT3
CCDC6, SCP2, POR"		SIRT3, CD44, HSPB1
TGFB1, CDCA3, "IL1B"		MPC1, SLC40A1, KDM4A
CTSB, CYBB, AGPAT3, MIOX		CDKN1A, PARP9, CBS
SAT1, SNX5, TIMP1, YAP1		CREB3, LCN2, SRSF9
RPL8, NDRG1, LPIN1		ARF6, TMSB4X, NQO1
ACADSB, ATF3, ACSL4		ECH1, IDH2, NFE2L2
AQP3, DPEP1, PGD		PARP14, MGST1
G6PDX, CPEB1, CYGB, CDO1		CISD1, FTH1, TMBIM4
TGFBR1, CFL1, CLTRN, ANO6		ISCU, NEDD4, SMPD1
PIEZO1, TOR2A, SMPD1		PARP3, RARRES2
MDM2, NOX4, HMGB1		ALDH3A2, CAV1
TIMM9, HMOX1, TNFAIP3		BCAT2, HMOX1, JUN
PTPN6, ATF4, DLD		NFS1, RBMS1, PARK7
SLC1A5, LONP1, MMD		ABHD12, ATF4, BRD2
AMN, GABARAPL1, TRIM26		P4HB, PARP2, ENPP2
MAP1LC3A, ACO1, ACSL1		SIRT6, CISD3, SLC3A2
SLC39A7, ELOVL5, EGR1		GALNT14, PLIN2, DECR1
MDM4, EGLN2, NCOA4		GPX4, DAZAP1, GLRX5
MAPK14, EPAS1, KLF2		PRDX6, PML, BRD4
FADS2, CIRBP, CD82		PTPN18, FADS2, GSTM1
MAP3K11, CS, DNAJB6		KLHDC3, FURIN, GDF15
MTCH1, PEBP1, PGRMC1		PRDX1, GCLC, ZFP36
		HSF1, ABCC5

**Table 2.** The top five genes are visualized using the Venn diagram

8		
Gene symbol	log FC	p Value
NOX4	-43.519	8.33E-05
ATF3	34.673	4.94E-06
MAPK14	-9.009	2.79E-03
TIMP1	73.195	1.58E-06
EGR1	64.558	1.78E-03

UUO group of GSE217654 (P<0.01), consistent with the result in a recent study [30], not significantly correlated with GPX4 (P>0.05), but correlated negatively with xCT (P<0.01), and ACSL4 (P<0.01) (Figure 3E, 3G). The Protein-Protein Interaction (PPI) map illustrates the high linkage of these five genes (Figure 3F). EGR1 expression positively correlated with fibrosis markers (Fibronectin, Collagen Type I, Collagen Type II), on the other hand, NOX4, ATF3, MAPK14 and TIMP1 proved to be negatively correlated with those (Figure 3H). The left figure in UUO forest shows the process of fitting the random forest algorithm model. In contrast, the right one depicts the ranking of each variable in terms of importance. The model's error rate stabilizes as the number of decision trees. NOX4, ACSL4, ATF3, and TIMP1 were ranked

from the highest to the lowest (**Figure 3I**), providing a comprehensive understanding of the core genes involved ferroptosis and RIF.

GO and KEGG analysis and molecular docking results

GO analysis exhibited significant enrichment of these genes in response to oxygen levels, hypoxia, and oxidative stress (Figure 4A). KEGG pathway analysis revealed that DEGs related to ferroptosis were enriched in pathways associated with ferroptosis, human cytomegalovirus infection, advanced glycation end-productsrecombinant advanced glycation end-products (AGE-RAGE) signaling in diabetic complications, fluid shear stress, atherosclerosis, hepatitis B, and cancer proteoglycans (Figure 4B). Notably, many ferroptosis-related DEGs were enriched in oxidative signaling and cross-presentation of the AGE-RAGE pathway in diabetic complications. The five genes were enriched in the AGE-RAGE signaling pathway in diabetic complications (most notable), the Gonadotropinreleasing hormone (GnRH) signaling pathway, and the alcoholic liver disease pathway (Figure 4F). The docking results indicated that CCG could bind to the active site of GPX4, ACSL4, and xCT. The hydrogen bond between curculigo-

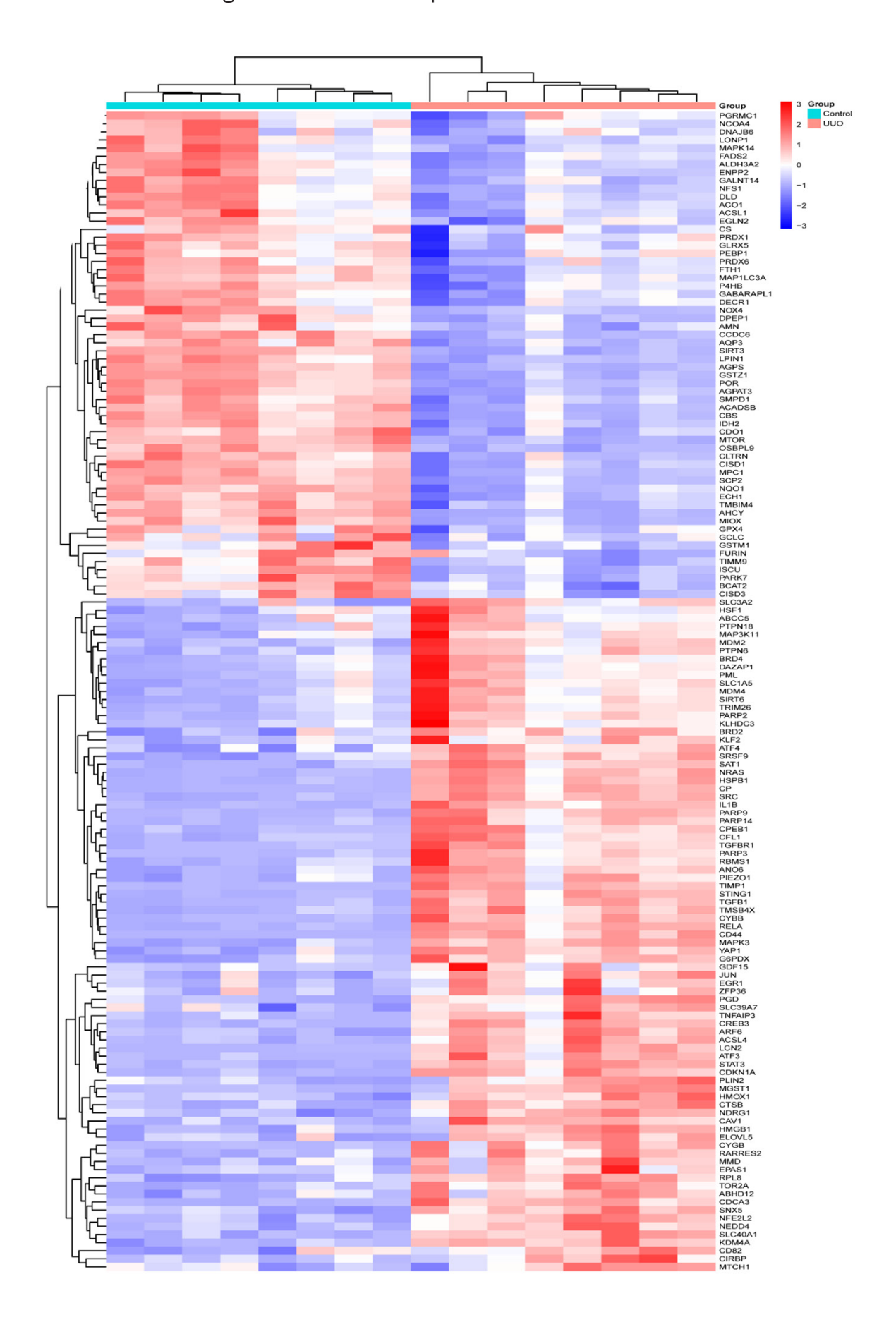


**Figure 2.** Heatmap of 143 ferroptosis-related differentially expressed genes (DEGs). These ferroptosis-related genes are downregulated in the blue groups and upregulated in the red ones. -3 to +3 is the expression value after z-score standardization, with negative values being reduced and positive values being increased.

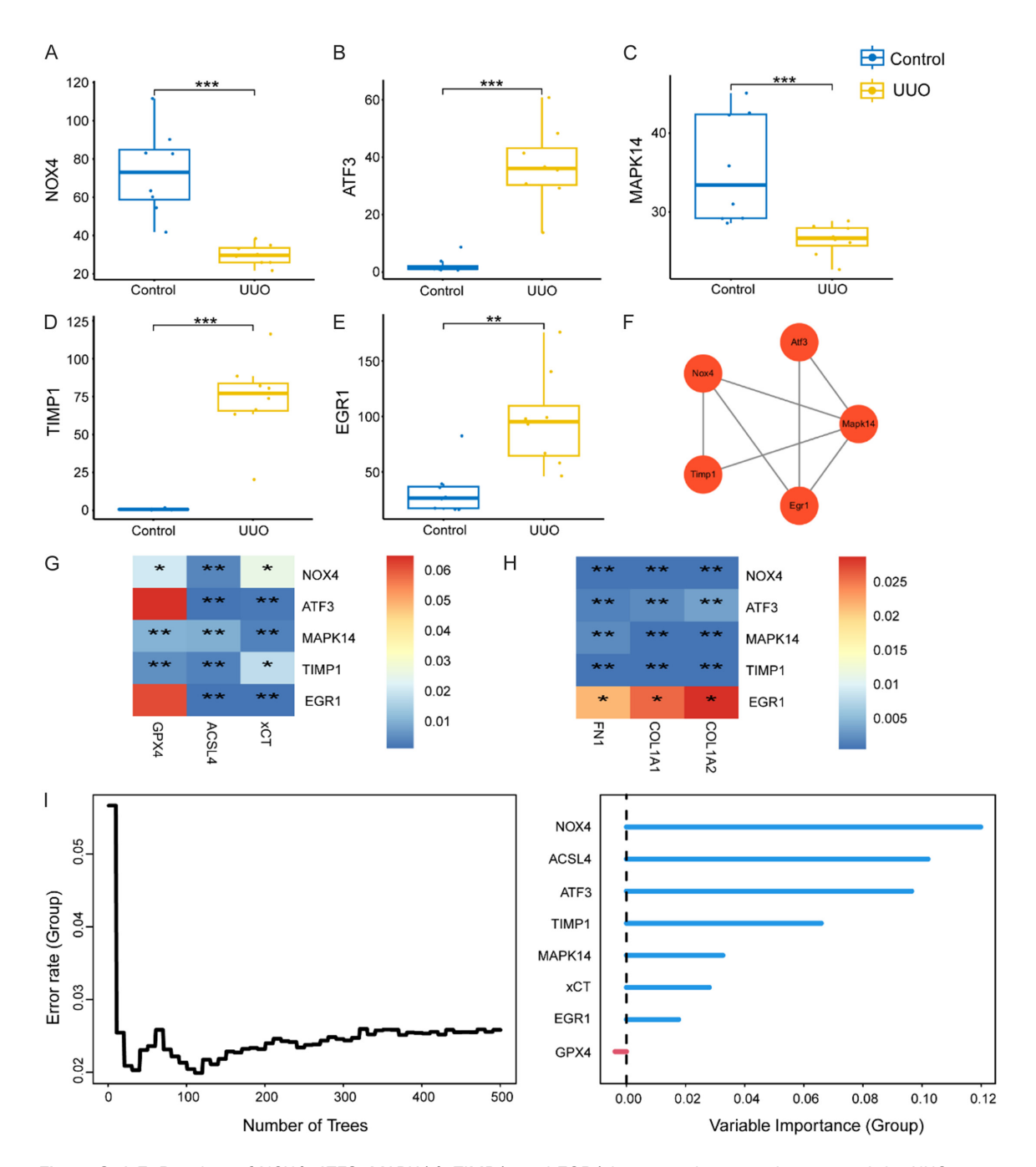


**Figure 3.** A-E. Boxplots of NOX4, ATF3, MAPK14, TIMP1, and EGR1 between the control group and the UUO group in GSE217654: The *p*-value \* is <0.05, \*\* is <0.01, \*\*\* is <0.001. F. Protein-Protein Interaction (PPI) of NOX4, ATF3, MAPK14, TIMP1, and EGR1. Red color represents that these genes are interconnected with each other and act with high intensity. G, H. Gene co-expression heatmaps. The Red color in the heatmap represents positively correlated, and blue color represents negatively correlated. The genes were valued by Spearman analysis. The r-value is between -1 and 1. I. The UUO Forest Importance. The left figure in the UUO forest shows the process of fitting the random forest algorithm model. In contrast, the right one depicts the ranking of each variable in terms of importance. The model's error rate stabilizes as the number of decision trees. NOX4, ACSL4, ATF3, and TIMP1 were ranked from the highest to the lowest F.

## Curculigoside alleviates ferroptosis in renal interstitial fibrosis

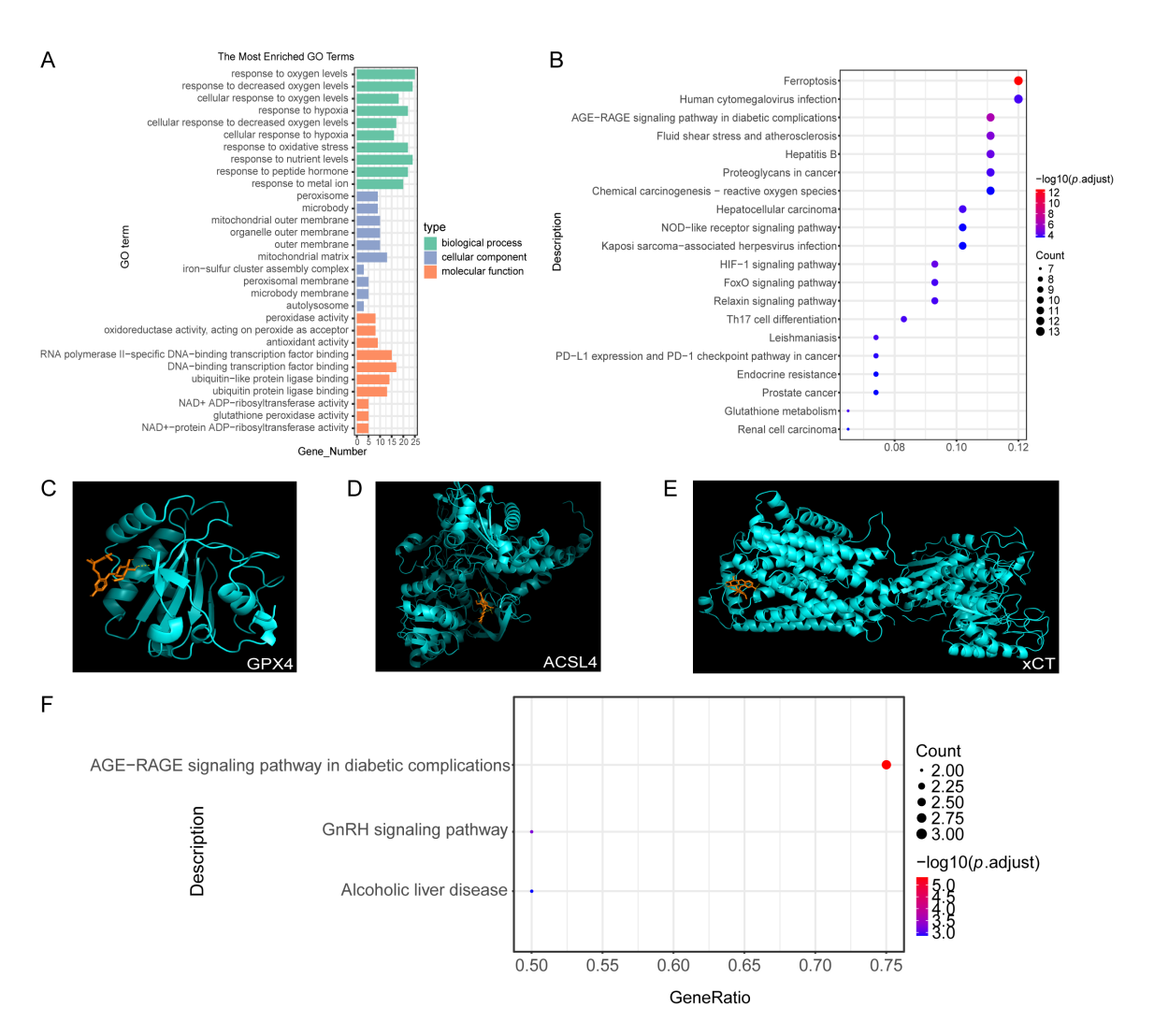


**Figure 4.** A. Enriched Gene Ontology (GO) terms (BP: biological process, MF: molecular function, and CC: cellular component) for ferroptosis-related DEGs in RIF. Node size reflects gene count, while node color (red to blue) indicates the significance of the *p*-value. B. Kyoto Encyclopedia of Genes and Genomes KEGG Pathway Enrichment Analysis Diagram. C-E. Molecular docking results of Curculigoside (CCG) interaction with Glutathione Peroxidase 4(GPX4), Acyl-COA Synthetase Long Chain Family Member 4(ACSL4), and Solute Carrier Family 7 Member 11 (Xct). F. KEGG-mapper: Gene ratio represents the proportion of genes enriched for this term; count represents the number of genes enriched; and P.adjust represents the corrected, logarithmized *p*-value. A *p*-value less than 0.05 was significant. A redder color represents a more critical pathway.

side and methyl (MET)-102 of GPX4 had a length of 2.3 A (**Figure 4C**), and the hydrogen bond between curculigoside and arginine (ARG)-340 of SLC7A11 had a length of 2.6 A (**Figure 4D**). Curculigoside formed hydrogen bonds with lysine (LYS)-113, valine (VAL)-114, and LYS-116 of ACSL4 (**Figure 4E**), with bond lengths of 2.4 A, 2.6 A, 2.2 A, and 2.4 A. The affinity values of CCG for GPX4, ACSL4, and xCT were -0.18, -0.98, and 0.01, derived from flexible docking, which allowed conformational adjustments of both the ligand and the protein's active site residues (**Table 3**). In normal

conditions, a docking binding energy of less than 0 kcal/mol suggests the presence of binding potential [31].

CCG improved kidney pathologic damage and downregulated the expression of fibrosis markers in UUO models

UUO models were established to mimic CKD *in vivo* and investigate whether CCG can improve kidney pathologic damage and fibrosis. H&E staining was employed to elucidate the morphology of kidney cells. Masson's trichrome

**Table 3.** Docking energy between CCG and ferroptosis-related proteins

Docking Protein	Binding Energy
GPX4	-0.18
SLC7A11	0.07
ACSL4	-0.98

staining was used to identify fibrous tissue represented by blue collagen. Compared to the sham group, the UUO group showed significant structural abnormalities of the kidney, particularly tubular dilation (Figure 5A-C). As renal interstitial fibrosis mainly occurs in the tubulointerstitium, our analysis focused on collagen deposition in the tubular region rather than in nephrons. Treatment with 5 mg/kg CCG significantly prevented the deposition of extracellular matrix (ECM) and tubular injury compared to UUO mice (Figure 5A-F). Compared to the UUO group, the area of collagen deposition was increased after treatment with ML385, which was reversed by 5 mg/kg CCG (Figure 5C-F). The levels of fibrotic proteins were significantly upregulated in the UUO model group. Notably, the expression levels of these proteins markedly decreased following treatment with 2.5 or 5 mg/kg CCG, particularly after treatment with 5 mg/kg CCG (Figure 5G-I). Pre-treatment with CCG significantly reduced the expression levels of fibrotic markers, suggesting its efficacy in mitigating RIF.

CCG suppressed the expression of ferroptosisrelated markers in the animal model of UUO

The relevant indices were evaluated to investigate the regulatory effects of CCG on ferroptosis. Compared to control subjects, immunohistochemical staining revealed a significant decrease in the expression of GPX4, xCT, and Nrf2 and an increase in the expression of ACS4 in UUO mice. These alterations were significantly reversed after treatment with 2.5 mg/kg and 5 mg/kg of CCG (Figure 6A-E). In the UUO group, the protein levels of GPX4, xCT, and Nrf2 were significantly elevated, whereas ACSL4 levels were significantly decreased compared to the sham group (Figure 6F-I). Western blotting demonstrated that CCG effectively reversed UUO-induced alterations in GPX4 and xCT expression and increased ACSL4 levels, with a notable effect observed in the 5 mg/kg CCG group (Figure 6F-I). Although CCG showed weak direct binding to xCT in docking, CCG-mediated upregulation of xCT (**Figure 6H**) may be due to Nrf2 activation, a known transcriptional regulator of SLC7A11. xCT upregulation reflects chronic adaptive responses to oxidative stress, whereas docking simulates acute binding events. These findings suggest that CCG may alleviate UUO-induced ferroptosis in animal models.

CCG and Fer-1 mitigated ferroptosis and oxidative stress in UUO models

To validate the effects of CCG on ferroptosis, it was compared with 5 mg/kg Fer-1, which is a classical and effective anti-ferroptosis agent [32]. Ferroptosis relies on the accumulation of intracellular iron and lipid peroxides [33]. We assessed the levels of intracellular iron. Superoxide dismutase (SOD) [34], glutathione (GSH) [35], and malondialdehyde (MDA) [36] in mouse kidney tissues. The results showed that 5 mg/kg CCG upregulated GPX4, xCT, and Nrf2 and downregulated ACSL4 in the UUO group, which was almost equal to the effect of 5 mg/ kg Fer-1 (Figure 7A-E). It was found that 5 mg/ kg CCG can notably enhance the expression of GPX4, xCT, and Nrf2 and reduce that of ACSL4 (Figure 7F-I). MDA and iron levels were upregulated in the UUO group, whereas GSH and SOD levels were downregulated compared to the sham group (Figure 7J-M). CCG (5 mg/kg) decreased MDA and iron levels and increased the concentrations of GSH and SOD (Figure **7J-M**). Therefore, it can be concluded that CCG possesses antioxidant properties that can protect against UUO-induced renal injury. We also found that the effects of CCG were comparable to those of Fer-1.

CCG modulated UUO-induced ferroptosis by regulating the Nrf2/HO-1 pathway

Nrf2 is a component of the antioxidant stress signaling pathway [37]. We focused on the Nrf2/HO-1 pathway to clarify the mechanism by which CCG modulates RIF. The Nrf2/HO-1 inhibitor, ML385, was used to determine whether CCG can activate this pathway. Immunohistochemical analysis revealed reduced expression levels of GPX4, xCT, and Nrf2 in the UUO group. This decrease was further exacerbated by ML385 but was rescued by 5 mg/kg of CCG (Figure 8A-E). The results indicated that Nrf2 and HO-1 levels decreased in the UUO group

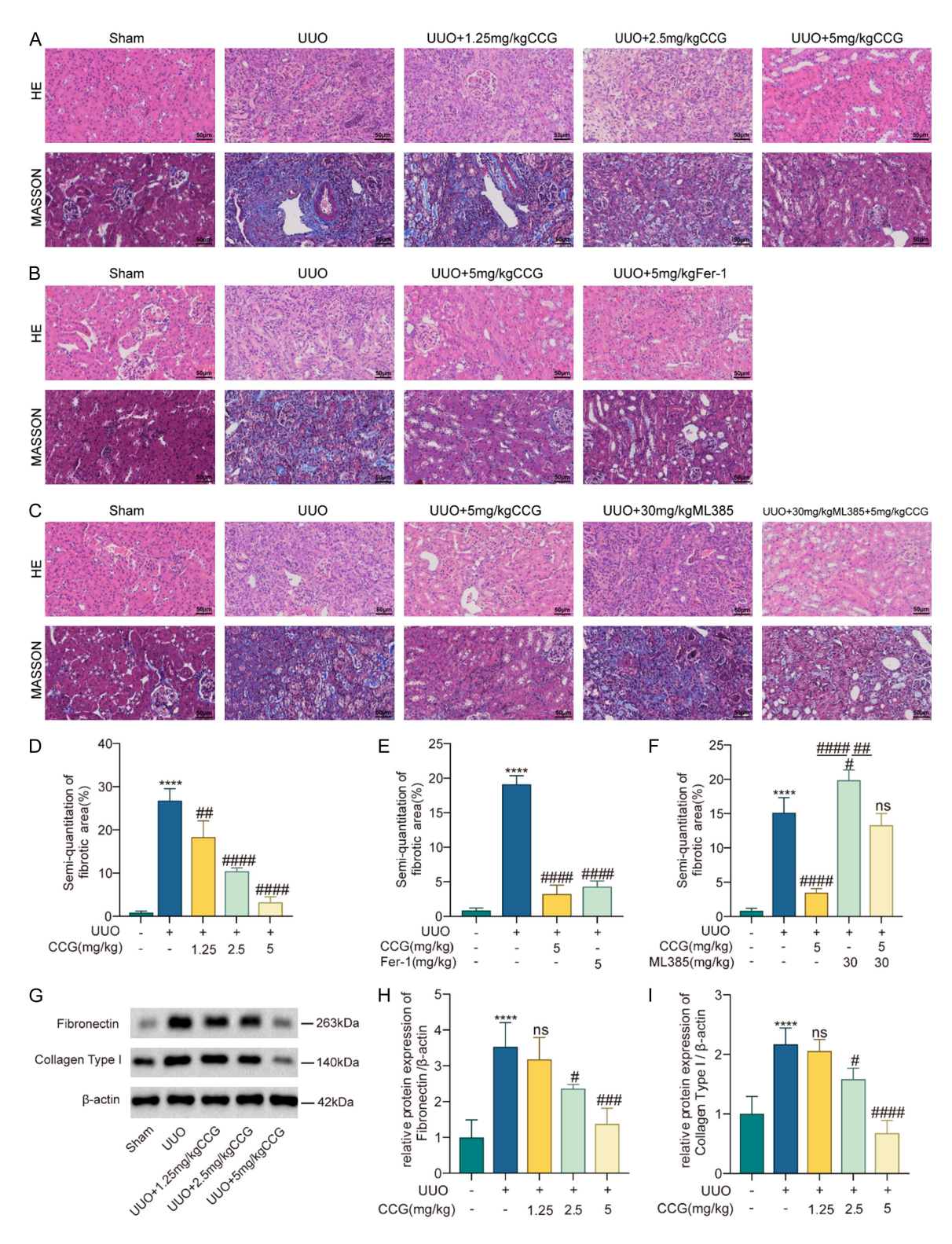
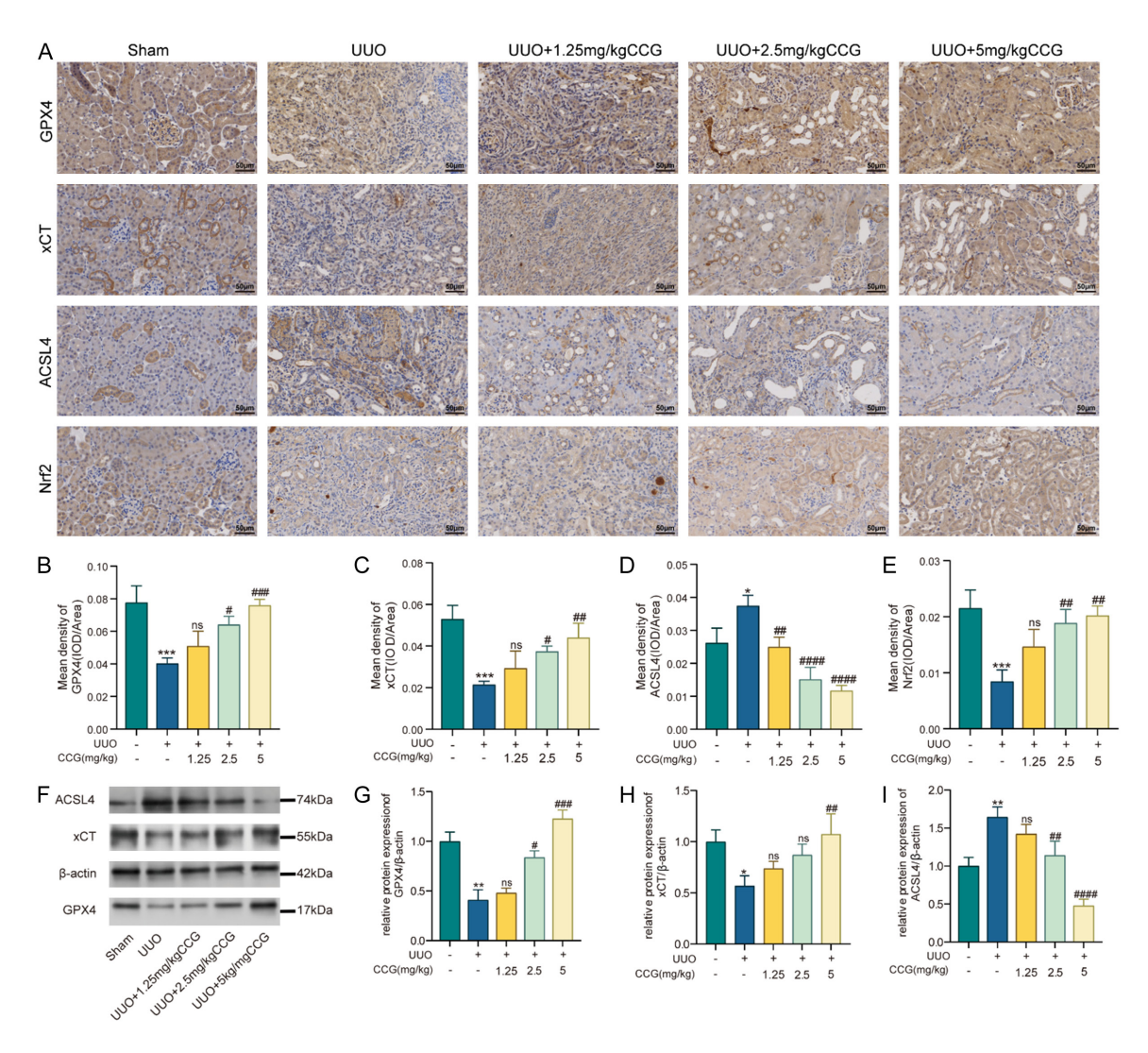


Figure 5. CCG alleviated kidney pathological damage and renal interstitial fibrosis in UUO models. A-C. Hematoxylin-Eosin (HE) staining was employed to assess the pathological alterations of the kidney. Masson staining was utilized to visualize renal fibrosis. (magnification 400×, scale bar 50  $\mu$ m). D-F. Semi-quantitative analysis of Masson staining. G. Western blotting was conducted to analyze the expression level of collagen type I and fibronectin in the kidney. H, I. Quantitative analysis of protein expression validated the effect of CCG (n=4). Values are shown as mean  $\pm$  SD (n=4). \* $^{P}$ <0.05, \* $^{P}$ <0.01, \* $^{P}$ <0.001, \* $^{P}$ <0.001 compared to the sham group; \* $^{P}$ <0.05, \* $^{P}$ <0.01, \* $^{P}$ <0.001, \* $^{P}$ <0.001 rs. the UUO group.



**Figure 6.** CCG suppressed the expression of ferroptosis-related proteins in the animal model of UUO. A. Immunohistochemical staining images in kidney tissues ( $400 \times$  magnification,  $50 \mu m$  scale bar). B-E. Quantitative measurement of average optical density. F. Western blotting was conducted to detect the expression levels of ferroptosis-related proteins after treatment with CCG. G-I. Quantitative analysis of the effect of CCG on the expression levels of GPX4, xCT, and ACSL4 proteins. (n=3). \*P<0.05, \*P<0.01, \*\*P<0.001, \*\*\*P<0.001 vs. the sham group; #P<0.01, \*\*P<0.01, \*\*\*P<0.01, \*\*P<0.01, \*

and increased in the CCG treatment group (Figure 8F-K), supporting the protective effects of CCG.

#### Discussion

Chronic kidney disease (CKD) is defined as a progressive decline in renal function, affecting approximately 10% of the global population, imposing significant challenges on families and society due to high morbidity and mortality rates [38]. Curculigoside, a phenolic glycoside compound, is recognized as the primary active ingredient of Curculigo orchioides [39].

Curculigoside possesses a wide range of pharmacologic properties, including antioxidant effects [15, 40], pro-angiogenesis properties [41], neuroprotective properties [42], and antiosteoporotic activities [43]. This study evaluated the protective significance of CCG in RIF using a mouse model of UUO. Our results demonstrated that CCG protects against ferroptosis and renal fibrosis through the Nrf2/HO-1 signaling pathway.

To investigate the pathogenesis of RIF, we analyzed gene sequencing data from UUO mice in the GEO database. KEGG and GO analyses

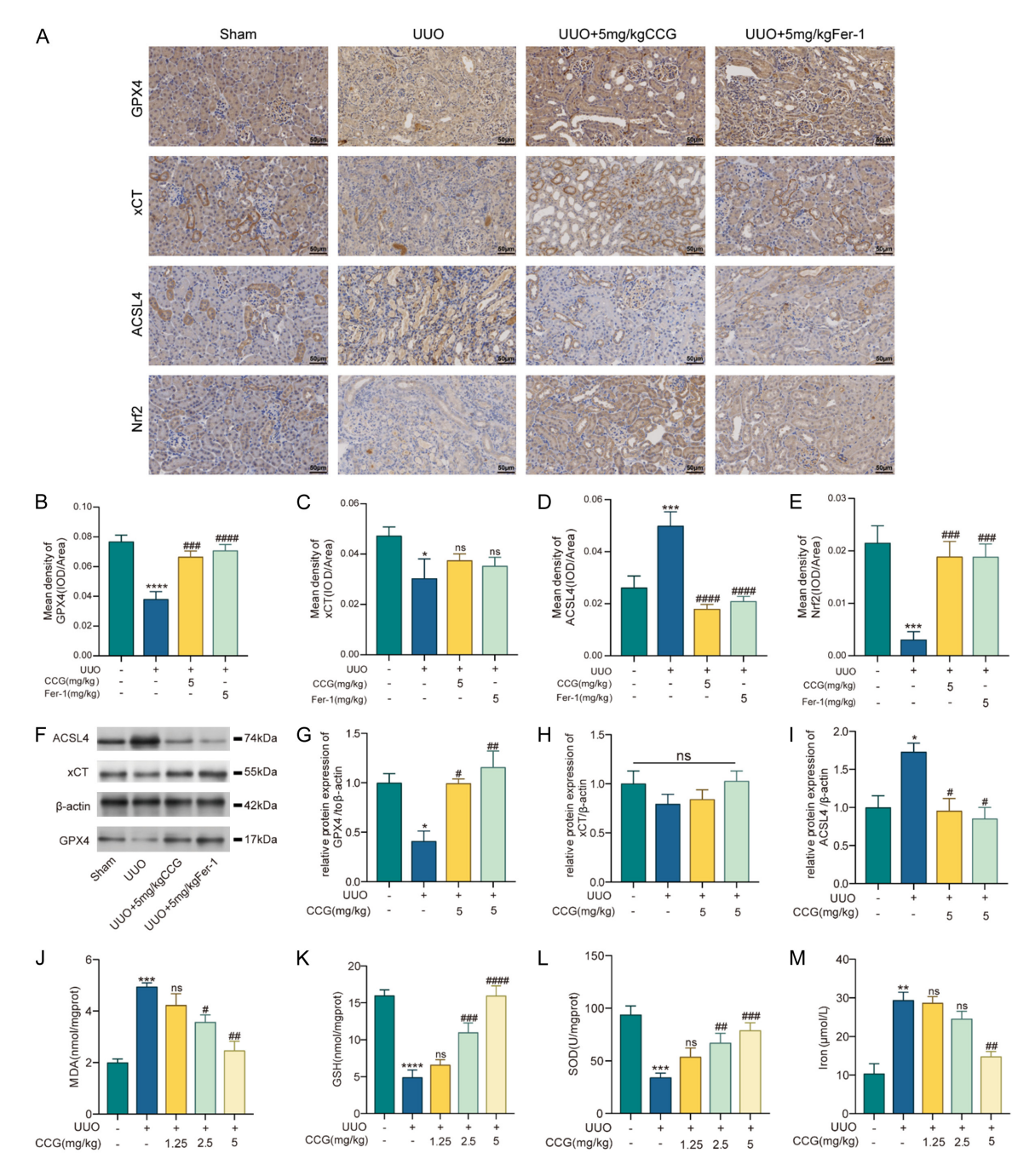


Figure 7. CCG and Fer-1 mitigated ferroptosis and oxidative stress in UUO models. A. Immunohistochemical staining images ( $400 \times$  magnification, 50 µm scale bar). B-E. Quantification of the mean optical density (n=3). F. Western blotting showing the effects of CCG and Fer-1 on ferroptosis. G-I. The quantitative assessment of the protein expression levels of GPX4, xCT, and ACSL4. J-M. Quantification of MDA, GSH, SOD, and iron levels (n=6). \*P<0.05, \*\*P<0.01, \*\*\*P<0.001 vs. the sham group; #P<0.05, ##P<0.01, ###P<0.001 vs. the UUO group.

revealed a close relationship between RIF and ferroptosis, with ferroptosis-related DEGs enriched in oxidative signaling. Five targets were identified, including NOX4, ATF3, MAPK14, TIMP1, and EGR1. Our findings regarding NOX4 were consistent with that of a recent study

which found that NOX4 expression was decreased in kidney samples of patients with chronic kidney disease [44]. Meanwhile, the expression of NOX4 is closely involved in the progression of DKD [23]. The appropriate activity of ATF3 is critical for cellular normal func-

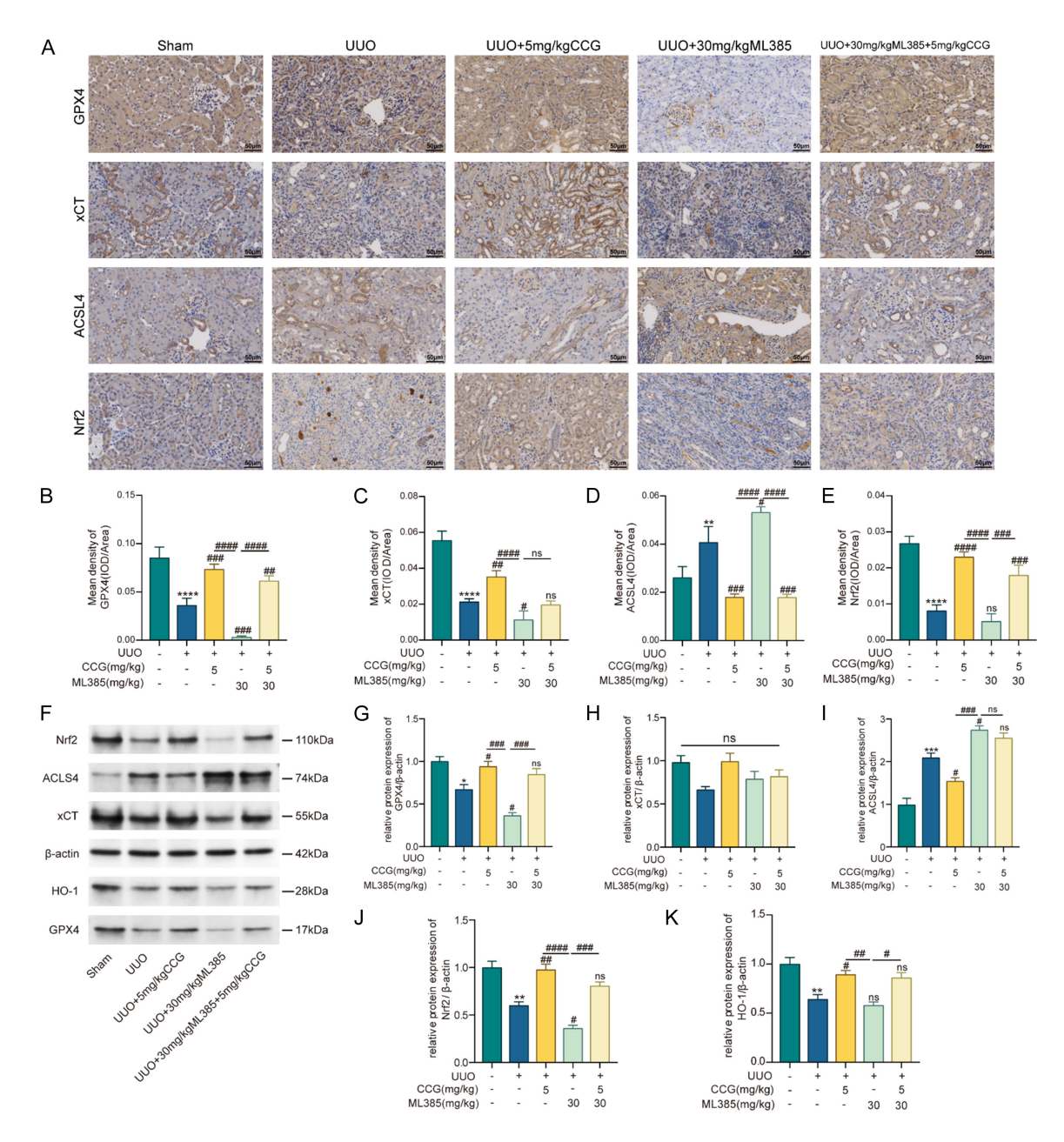


Figure 8. CCG regulated UUO-induced ferroptosis through the Nuclear factor erythroid 2-related factor 2(Nrf2)/heme oxygenase-1(HO-1) pathway. A. Immunohistochemical staining images of kidney tissues (magnification  $400\times$ , scale bar 50 µm). B-E. Quantification of average optical density. F. Western blotting showing the expression levels of ferroptosis-related proteins after treatment with ML385. G-K. The relative expression levels of GPX4, xCT, ACSL4, HO-1, and Nrf2 proteins (n=3). \*P<0.05, \*P<0.01, \*\*P<0.001 vs. the sham group; \*P<0.05, \*P<0.01, \*P<0.001, \*P<0.001 vs. the UUO group.

tions, and its abnormality induces pathophysiologic responses, including apoptosis, oxidative stress, and inflammation [45]. ATF3 can suppress the expression of SLC7A11, thereby promoting ferroptosis [46], consistent with the relationship between ATF3 and xCT in our study. MAPK14 may be related to the body's immunity and inflammation [47] and may drive

ferroptosis through the TP53/SLC7A11/GPX4 pathway [48]. In our research, MAPK14 was found to be downregulated in the UUO group, which is inconsistent with the findings of GSE15072 analysis [49]. Few studies have reported the role of MAPK14 in renal fibrosis and measured its correlation with ferroptosis; therefore, more studies are urgently needed to

unravel this detailed relationship. Plasma levels of TIMP1 have been reported to be associated with early diabetic nephropathy in patients with type 1 diabetes [50]. Our findings were consistent with those of previous studies [51, 52] regarding TIMP1. EGR1 upregulation in the UUO group and its correlation with ferroptosis markers were consistent with the results of previous studies [53, 54]. Based on the enrichment and core gene analysis of ferroptosisrelated DEGs, machine learning revealed that NOX4, ACSL4, ATF3, and TIMP1, the four genes ranked as essential genes, wrere associated with both ferroptosis and fibrosis. This strengthens the relationship between ferroptosis and RIF. These five genes were enriched in the AGE-RAGE signaling pathway in diabetic complications, commonly associated with ferroptosis. Although we identified these five genes as hub genes linking ferroptosis to RIF, their precise mechanistic roles require further validation using genetic models.

Molecular docking results revealed that CCG can bind to GPX4 and ACSL4. Although our docking results suggested strong binding affinity, the absence of full protein flexibility simulations may have underestimated conformational changes upon ligand binding. CCG revealed binding affinity to GPX4 and ACSL4, but molecular docking suggested weak direct interaction between CCG and xCT, and its protein upregulation indicated potential indirect mechanisms. This discrepancy may arise from two factors: 1) the binding of CCG to upstream regulators (e.g., Nrf2) rather than xCT itself, and 2) post-translational stabilization of the xCT protein by CCGmediated redox modulation. Future studies should integrate MD simulations to validate these interactions.

Given the minimal side effects of TCM, this study investigated the efficacy of CCG and its mechanism in the treatment of RIF. Histopathologic examinations revealed that kidneys in the UUO group exhibited significant enlargement and edema. Extensive tissue damage was predominantly observed in the renal medulla, leading to tubular necrosis, congestive hemorrhage, and protein casts. These findings are consistent with those of previous studies [55, 56]. Fibrogenic stimuli induce oxidative stress in the kidneys during the early phase, activating various fibrotic responses [57]. Western blotting indicated that CCG downregu-

lated fibrosis-related proteins in a dose-dependent manner, indicating potential efficacy of CCG for treating RIF.

Ferroptosis has been linked to various diseases associated with oxidative imbalance [58]. Targeting ferroptosis is a promising strategy for treating chronic diseases, including CKD [59]. Inhibition of GPX4 leads to a ferroptotic cascade [60]. GPX4 eliminates ROS and is converted into glutathione disulfide (GSSG) through the oxidation of GSH, a coenzyme that contributes to lipid peroxidation [43, 61-64]. xCT mitigates ferroptosis under iron overload conditions [65, 66]. The biosynthesis of arachidonoyl-CoA, catalyzed by ACSL4, plays a crucial role in ferroptosis [67]. Immunohistochemistry results and western blot analyses in our study showed that CCG decreased GPX4 and xCT levels and increased ACSL4. Consistently, in vitro experiments have demonstrated that inhibition of ferroptosis or ACSL4 mitigates renal fibrosis [68]. Knockdown of ACSL4 effectively attenuated the interstitial fibrotic response [69], suggesting further research on the genetic modification of ACSL4 at the gene level. Our FerrDbbased analysis suggested that ferroptosis activation in RIF is driven by upregulation of proferroptotic drivers (e.g., ACSL4) and loss of ferroptosis suppressors (e.g., GPX4), forming a 'two-hit' mechanism that accelerates tubular injury and renal fibrosis. We evaluated oxidative stress markers, such as GSH, SOD, and MDA, in kidney tissues. Compared to the sham group, UUO mice exhibited significantly decreased GSH and SOD activities, as well as elevated levels of MDA and iron, which reflect substantial renal damage. CCG exhibited greater effects compared to the classic ferroptosis inhibitor Fer-1 [32]. Our results confirmed that 5 mg/kg CCG significantly inhibited fibrosis and downregulated the expression of proteins associated with ferroptosis, consistent with the findings of Luo et al [70]. Treatment with CCG significantly increased GSH and SOD activity and decreased MDA and iron levels, suggesting that CCG effectively suppressed oxidative stress in RIF.

The Nrf2/ARE signaling pathway is a key pathway that significantly enhances the expression of HO-1, thereby attenuating oxidative stress [20]. Regulation of ferroptosis, primarily through the Nrf2 pathway, is crucial for maintaining cellular redox balance and suppressing ferroptosis

[71-74]. This study observed decreased Nrf2 expression in the UUO group, consistent with the findings of previous studies on RIF and ferroptosis [75, 76]. We observed a reduced expression level of HO-1 and Nrf2 in kidney tissues after UUO, with partial recovery following treatment with CCG, consistent with previous findings on the Nrf2 inhibitor, ML385 [77]. This finding suggests that CCG can alleviate UUO-induced oxidative stress through the Nrf2/HO-1 pathway.

This study demonstrated that CCG mitigated fibrosis and renal oxidative stress injury by modulating Nrf2 signaling pathways. As a limitation, *in vitro* findings of this study cannot be directly extrapolated to clinical observations regarding the application of CCG in the treatment of RIF. Future studies should provide a more comprehensive theoretical foundation for the clinical use of CCG in managing RIF. Understanding the pathophysiologic mechanisms and clinical significance of ferroptosis will enable targeted strategies for the management of kidney diseases.

## Acknowledgements

The work was supported by a grant from the National Natural Science Foundation of China (No. 81670659).

## Disclosure of conflict of interest

None.

Address correspondence to: Rujuan Xie, Department of Nephrology, The First Affiliated Hospital of Harbin Medical University, Harbin 150000, Heilongjiang, China. E-mail: xierj@hrbmu.edu.cn

## References

- [1] Jing H, Tang S, Lin S, Liao M, Chen H, Fan Y and Zhou J. Adiponectin in renal fibrosis. Aging (Albany NY) 2020; 12: 4660-4672.
- [2] Liang GQ, Mu W and Jiang CB. Baicalein improves renal interstitial fibrosis by inhibiting the ferroptosis in vivo and in vitro. Heliyon 2024; 10: e28954.
- [3] Olinger E, Phakdeekitcharoen P, Caliskan Y, Orr S, Mabillard H, Pickles C, Tse Y and Wood K; Genomics England Research Consortium, Sayer JA. Biallelic variants in TTC21B as a rare cause of early-onset arterial hypertension and tubuloglomerular kidney disease. Am J Med

- Genet C Semin Med Genet 2022; 190: 109-120.
- [4] Chen DQ, Chen L, Guo Y, Wu XQ, Zhao TT, Zhao HL, Zhang HJ, Yan MH, Zhang GQ and Li P. Poricoic acid A suppresses renal fibroblast activation and interstitial fibrosis in UUO rats via upregulating Sirt3 and promoting β-catenin K49 deacetylation. Acta Pharmacol Sin 2023; 44: 1038-1050.
- [5] Wu R, Li J, Tu G, Su Y, Zhang X, Luo Z, Rong R and Zhang Y. Comprehensive molecular and cellular characterization of acute kidney injury progression to renal fibrosis. Front Immunol 2021; 12: 699192.
- [6] Neyra JA and Chawla LS. Acute kidney disease to chronic kidney disease. Crit Care Clin 2021; 37: 453-474.
- [7] Wang P, Chen W, Li B, Yang S, Li W, Zhao S, Ning J, Zhou X and Cheng F. Exosomes on the development and progression of renal fibrosis. Cell Prolif 2024; 57: e13677.
- [8] Li X, Ma TK, Wang P, Shi H, Hai S, Qin Y, Zou Y, Zhu WT, Li HM, Li YN, Yin L, Xu YY, Yang Q, Zhang S and Ding H. HOXD10 attenuates renal fibrosis by inhibiting NOX4-induced ferroptosis. Cell Death Dis 2024; 15: 398.
- [9] Chen L, Xu H, Zhang C, He J and Wang Y. Semaglutide alleviates early brain injury following subarachnoid hemorrhage by suppressing ferroptosis and neuroinflammation via SIRT1 pathway. Am J Transl Res 2024; 16: 1102-1117.
- [10] Shi Y, Shi X, Zhao M, Zhang Y, Zhang Q, Liu J, Duan H, Yang B and Zhang Y. Ferroptosis is involved in focal segmental glomerulosclerosis in rats. Sci Rep 2023; 13: 22250.
- [11] Song Q, Peng S, Che F and Zhu X. Artesunate induces ferroptosis via modulation of p38 and ERK signaling pathway in glioblastoma cells. J Pharmacol Sci 2022; 148: 300-306.
- [12] Yang Z, He K, Chen W and Chen Y. A ferroptosis-related ceRNA network in hepatocellular carcinoma for potential clinical applications. Am J Transl Res 2023; 15: 3912-3927.
- [13] Chen Y, Zhang F, Sun J and Zhang L. Identifying the natural products in the treatment of atherosclerosis by increasing HDL-C level based on bioinformatics analysis, molecular docking, and in vitro experiment. J Transl Med 2023; 21: 920.
- [14] You WL and Xu ZL. Curculigoside promotes osteogenic differentiation of ADSCs to prevent ovariectomized-induced osteoporosis. J Orthop Surg Res 2021; 16: 279.
- [15] Xie W, Deng L, Qian R, Huang X, Liu W and Tang S. Curculigoside attenuates endoplasmic reticulum stress-induced epithelial cell and fibroblast senescence by regulating the SIRT1-P300

- signaling pathway. Antioxidants (Basel) 2024; 13: 420.
- [16] Li F, Huang H, Zhao P, Jiang J, Ding X, Lu D and Ji L. Curculigoside mitigates dextran sulfate sodium-induced colitis by activation of KEAP1-NRF2 interaction to inhibit oxidative damage and autophagy of intestinal epithelium barrier. Int J Mol Med 2023; 52: 107.
- [17] He T, Huang J, Peng B, Wang M, Shui Q and Cai L. Screening of potential biomarkers in propofol-induced neurotoxicity via bioinformatics prediction and experimental verification. Am J Transl Res 2024; 16: 755-767.
- [18] Nogales C, Mamdouh ZM, List M, Kiel C, Casas Al and Schmidt HHHW. Network pharmacology: curing causal mechanisms instead of treating symptoms. Trends Pharmacol Sci 2022; 43: 136-150.
- [19] Stancic A, Velickovic K, Markelic M, Grigorov I, Saksida T, Savic N, Vucetic M, Martinovic V, Ivanovic A and Otasevic V. Involvement of ferroptosis in diabetes-induced liver pathology. Int J Mol Sci 2022; 23: 9309.
- [20] Zhang Q, Liu J, Duan H, Li R, Peng W and Wu C. Activation of Nrf2/HO-1 signaling: an important molecular mechanism of herbal medicine in the treatment of atherosclerosis via the protection of vascular endothelial cells from oxidative stress. J Adv Res 2021; 34: 43-63.
- [21] Li J, Lu K, Sun F, Tan S, Zhang X, Sheng W, Hao W, Liu M, Lv W and Han W. Panaxydol attenuates ferroptosis against LPS-induced acute lung injury in mice by Keap1-Nrf2/H0-1 pathway. J Transl Med 2021; 19: 96.
- [22] Li J, Yang J, Xian Q, Su H, Ni Y and Wang L. Kaempferitrin attenuates unilateral ureteral obstruction-induced renal inflammation and fibrosis in mice by inhibiting NOX4-mediated tubular ferroptosis. Phytother Res 2024; 38: 2656-2668.
- [23] Ji P, Shi Q, Liu Y, Han M, Su Y, Sun R, Zhou H, Li W and Li W. Ginsenoside Rg1 treatment alleviates renal fibrosis by inhibiting the NOX4-MAPK pathway in T2DM mice. Ren Fail 2023; 45: 2197075.
- [24] Tang Q, Li J, Wang Y and Sun Q. Identification and verification of hub genes associated with ferroptosis in ischemia and reperfusion injury during renal transplantation. Int Immunopharmacol 2023; 120: 110393.
- [25] Fu D, Wang C, Yu L and Yu R. Induction of ferroptosis by ATF3 elevation alleviates cisplatin resistance in gastric cancer by restraining Nrf2/Keap1/xCT signaling. Cell Mol Biol Lett 2021; 26: 26.
- [26] Liu J, Yu X, Yu H, Liu B, Zhang Z, Kong C and Li Z. Knockdown of MAPK14 inhibits the proliferation and migration of clear cell renal cell car-

- cinoma by downregulating the expression of CDC25B. Cancer Med 2020; 9: 1183-1195.
- [27] Rao J, Wang T, Wang K and Qiu F. Integrative analysis of metabolomics and proteomics reveals mechanism of berberrubine-induced nephrotoxicity. Toxicol Appl Pharmacol 2024; 488: 116992.
- [28] Dagar N, Jadhav HR and Gaikwad AB. Network pharmacology combined with molecular docking and dynamics to assess the synergism of esculetin and phloretin against acute kidney injury-diabetes comorbidity. Mol Divers 2025; 29: 1-19.
- [29] Guo A, Wang W, Shi H, Wang J and Liu T. Identification of hub genes and pathways in a rat model of renal ischemia-reperfusion injury using bioinformatics analysis of the gene expression omnibus (GEO) dataset and integration of gene expression profiles. Med Sci Monit 2019; 25: 8403-8411.
- [30] Ai K, Li X, Zhang P, Pan J, Li H, He Z, Zhang H, Yi L, Kang Y, Wang Y, Chen J, Li Y, Xiang X, Chai X and Zhang D. Genetic or siRNA inhibition of MBD2 attenuates the UUO- and I/R-induced renal fibrosis via downregulation of EGR1. Mol Ther Nucleic Acids 2022; 28: 77-86.
- [31] Guedes IA, de Magalhães CS and Dardenne LE. Receptor-ligand molecular docking. Biophys Rev 2014; 6: 75-87.
- [32] Xie J, Ye Z, Li L, Xia Y, Yuan R, Ruan Y and Zhou X. Ferrostatin-1 alleviates oxalate-induced renal tubular epithelial cell injury, fibrosis and calcium oxalate stone formation by inhibiting ferroptosis. Mol Med Rep 2022; 26: 256.
- [33] Wu H, Liu Q, Shan X, Gao W and Chen Q. ATM orchestrates ferritinophagy and ferroptosis by phosphorylating NCOA4. Autophagy 2023; 19: 2062-2077.
- [34] Radavi-Asgar M, Sabet N, Khaksari M, Jafari E, Soltani Z and Dehghanian F. The prescription of oral mucosal mesenchymal stem cells post-traumatic brain injury improved the kidney and heart inflammation and oxidative stress. Biomed Res Int 2022; 2022: 8235961.
- [35] Qin Y, Qiao Y, Wang D, Tang C and Yan G. Ferritinophagy and ferroptosis in cardiovascular disease: mechanisms and potential applications. Biomed Pharmacother 2021; 141: 111872.
- [36] Yui K, Imataka G and Shiohama T. Lipid peroxidation of the docosahexaenoic acid/arachidonic acid ratio relating to the social behaviors of individuals with autism spectrum disorder: the relationship with ferroptosis. Int J Mol Sci 2023; 24: 14796.
- [37] Zhang X, Yang F, Zhang Y, Song X, Xue S, Chang Y, Zhong Y, Dou Y and Wang Y. Modified Buyang huanwu decoction alleviates diabetic liver in-

- jury via inhibiting oxidative stress in db/db mice. Am J Transl Res 2024; 16: 39-50.
- [38] Miguel V and Kramann R. Metabolic reprogramming heterogeneity in chronic kidney disease. FEBS Open Bio 2023; 13: 1154-1163.
- [39] Wang A, Ning J, Zhao L and Xu R. Lipid-lowering effect and oral transport characteristics study of curculigoside. Front Cardiovasc Med 2024; 11: 1426379.
- [40] Fan J and Watanabe T. Atherosclerosis: known and unknown. Pathol Int 2022; 72: 151-160.
- [41] Zhu Y, Yang H, Han L, Mervin LH, Hosseini-Gerami L, Li P, Wright P, Trapotsi MA, Liu K, Fan TP and Bender A. In silico prediction and biological assessment of novel angiogenesis modulators from traditional Chinese medicine. Front Pharmacol 2023; 14: 1116081.
- [42] Wang Y, Liu Z, Wei J, Di L, Wang S, Wu T and Li N. Norlignans and phenolics from genus Curculigo protect corticosterone-injured neuroblastoma cells SH-SY5Y by inhibiting endoplasmic reticulum stress-mitochondria pathway. J Ethnopharmacol 2022; 296: 115430.
- [43] Wang N, Li Z, Li S, Li Y, Gao L, Bao X, Wang K, Liu C, Xue P and Liu S. Curculigoside ameliorates bone loss by influencing mesenchymal stem cell fate in aging mice. Front Cell Dev Biol 2021; 9: 767006.
- [44] Jiménez-Uribe AP, Gómez-Sierra T, Aparicio-Trejo OE, Orozco-Ibarra M and Pedraza-Chaverri J. Backstage players of fibrosis: NOX4, mTOR, HDAC, and S1P; companions of TGF-β. Cell Signal 2021; 87: 110123.
- [45] Feng J, Li Y, Jin X, Gong R and Xia Z. ATF3 regulates oxidative stress and extracellular matrix degradation via p38/Nrf2 signaling pathway in pelvic organ prolapse. Tissue Cell 2021; 73: 101660.
- [46] Wang L, Liu Y, Du T, Yang H, Lei L, Guo M, Ding HF, Zhang J, Wang H, Chen X and Yan C. ATF3 promotes erastin-induced ferroptosis by suppressing system Xc. Cell Death Differ 2020; 27: 662-675.
- [47] Chen Y, Lu M, Lin M and Gao Q. Network pharmacology and molecular docking to elucidate the common mechanism of hydroxychloroquine treatment in lupus nephritis and IgA nephropathy. Lupus 2024; 33: 347-356.
- [48] Zhang N, Fan Y, Chen J, Gu J and Yan X. MAPK14 drives Ferroptosis and immune dysfunction in pediatric Sepsis-induced acute lung injury. Cell Immunol 2025; 411-412: 104948.
- [49] Shao L, Fang Q, Ba C, Zhang Y, Shi C, Zhang Y and Wang J. Identification of ferroptosis-associated genes in chronic kidney disease. Exp Ther Med 2023; 25: 60.
- [50] Papadopoulou-Marketou N, Whiss PA, Eriksson AC, Hyllienmark L, Papassotiriou I and

- Wahlberg J. Plasma levels of tissue inhibitor of metalloproteinase-1 in patients with type 1 diabetes mellitus associate with early diabetic neuropathy and nephropathy. Diab Vasc Dis Res 2021; 18: 14791641211002470.
- [51] Hu Z, Liu Y, Zhu Y, Cui H and Pan J. Identification of key biomarkers and immune infiltration in renal interstitial fibrosis. Ann Transl Med 2022; 10: 190.
- [52] Lee JA, Shin MR and Roh SS. Corni fructus alleviates UUO-induced renal fibrosis via TGF-β/ Smad signaling. Biomed Res Int 2022; 2022: 5780964.
- [53] Stepanova G, Manzéger A, Mózes MM and Kökény G. Renal epithelial complement C3 expression affects kidney fibrosis progression. Int J Mol Sci 2024; 25: 12551.
- [54] Wang Y, Shen Z, Mo S, Zhang H, Chen J, Zhu C, Lv S, Zhang D, Huang X, Gu Y, Yu X, Ding X and Zhang X. Crosstalk among proximal tubular cells, macrophages, and fibroblasts in acute kidney injury: single-cell profiling from the perspective of ferroptosis. Hum Cell 2024; 37: 1039-1055.
- [55] Martínez-Klimova E, Aparicio-Trejo OE, Tapia E and Pedraza-Chaverri J. Unilateral ureteral obstruction as a model to investigate fibrosis-attenuating treatments. Biomolecules 2019; 9: 141.
- [56] Shu G, Yusuf A, Dai C, Sun H and Deng X. Piperine inhibits AML-12 hepatocyte EMT and LX-2 HSC activation and alleviates mouse liver fibrosis provoked by CCl(4): roles in the activation of the Nrf2 cascade and subsequent suppression of the TGF-β1/Smad axis. Food Funct 2021; 12: 11686-11703.
- [57] Chen YC, Chen JH, Tsai CF, Wu CY, Chang CN, Wu CT and Yeh WL. Protective effects of paeonol against cognitive impairment in lung diseases. J Pharmacol Sci 2024; 155: 101-112.
- [58] Mohan S, Alhazmi HA, Hassani R, Khuwaja G, Maheshkumar VP, Aldahish A and Chidambaram K. Role of ferroptosis pathways in neuroinflammation and neurological disorders: from pathogenesis to treatment. Heliyon 2024; 10: e24786.
- [59] Song J, Wang H, Sheng J, Zhang W, Lei J, Gan W, Cai F and Yang Y. Vitexin attenuates chronic kidney disease by inhibiting renal tubular epithelial cell ferroptosis via NRF2 activation. Mol Med 2023; 29: 147.
- [60] Wang C, Liu T, Tong Y, Cui R, Qu K, Liu C and Zhang J. Ulinastatin protects against acetaminophen-induced liver injury by alleviating ferroptosis via the SIRT1/NRF2/HO-1 pathway. Am J Transl Res 2021; 13: 6031-6042.
- [61] Hosohata K, Harnsirikarn T and Chokesuwattanaskul S. Ferroptosis: a potential therapeutic

## Curculigoside alleviates ferroptosis in renal interstitial fibrosis

- target in acute kidney injury. Int J Mol Sci 2022; 23: 6583.
- [62] Yan HF, Zou T, Tuo QZ, Xu S, Li H, Belaidi AA and Lei P. Ferroptosis: mechanisms and links with diseases. Signal Transduct Target Ther 2021; 6: 49.
- [63] Liu J, Kang R and Tang D. Signaling pathways and defense mechanisms of ferroptosis. FEBS J 2022; 289: 7038-7050.
- [64] Chen T, Ding L, Zhao M, Song S, Hou J, Li X, Li M, Yin K, Li X and Wang Z. Recent advances in the potential effects of natural products from traditional Chinese medicine against respiratory diseases targeting ferroptosis. Chin Med 2024; 19: 49.
- [65] Zhang J, Wang X, Guan B, Wang X, An X, Wang T, Chen X, Zhao L, Jia J, Song L, Ma D, Li Q, Zhang H, Ju J and Xu H. Qing-Xin-Jie-Yu Granule inhibits ferroptosis and stabilizes atherosclerotic plaques by regulating the GPX4/xCT signaling pathway. J Ethnopharmacol 2023; 301: 115852.
- [66] Ashraf A, Jeandriens J, Parkes HG and So PW. Iron dyshomeostasis, lipid peroxidation and perturbed expression of cystine/glutamate antiporter in Alzheimer's disease: evidence of ferroptosis. Redox Biol 2020; 32: 101494.
- [67] Ding K, Liu C, Li L, Yang M, Jiang N, Luo S and Sun L. Acyl-CoA synthase ACSL4: an essential target in ferroptosis and fatty acid metabolism. Chin Med J (Engl) 2023; 136: 2521-2537.
- [68] Li L, Ye Z, Xia Y, Li B, Chen L, Yan X, Yuan T, Song B, Yu W, Rao T, Lin F, Zhou X and Cheng F. YAP/ACSL4 pathway-mediated ferroptosis promotes renal fibrosis in the presence of kidney stones. Biomedicines 2023; 11: 2692.
- [69] Dai Y, Chen Y, Mo D, Jin R, Huang Y, Zhang L, Zhang C, Gao H and Yan Q. Inhibition of ACSL4 ameliorates tubular ferroptotic cell death and protects against fibrotic kidney disease. Commun Biol 2023; 6: 907.

- [70] Luo Y, Chen H, Liu H, Jia W, Yan J, Ding W, Zhang Y, Xiao Z and Zhu Z. Protective effects of ferroptosis inhibition on high fat diet-induced liver and renal injury in mice. Int J Clin Exp Pathol 2020; 13: 2041-2049.
- [71] He F, Ru X and Wen T. NRF2, a transcription factor for stress response and beyond. Int J Mol Sci 2020; 21: 4777.
- [72] Baird L and Yamamoto M. The molecular mechanisms regulating the KEAP1-NRF2 pathway. Mol Cell Biol 2020; 40: e00099-20.
- [73] Dodson M, Castro-Portuguez R and Zhang DD. NRF2 plays a critical role in mitigating lipid peroxidation and ferroptosis. Redox Biol 2019; 23: 101107.
- [74] Kerins MJ and Ooi A. The roles of NRF2 in modulating cellular iron homeostasis. Antioxid Redox Signal 2018; 29: 1756-1773.
- [75] Zhou L, Xue X, Hou Q and Dai C. Targeting ferroptosis attenuates interstitial inflammation and kidney fibrosis. Kidney Dis (Basel) 2021; 8: 57-71.
- [76] Zhu B, Ni Y, Gong Y, Kang X, Guo H, Liu X, Li J and Wang L. Formononetin ameliorates ferroptosis-associated fibrosis in renal tubular epithelial cells and in mice with chronic kidney disease by suppressing the Smad3/ATF3/SL-C7A11 signaling. Life Sci 2023; 315: 121331.
- [77] Xian P, Hei Y, Wang R, Wang T, Yang J, Li J, Di Z, Liu Z, Baskys A, Liu W, Wu S and Long Q. Mesenchymal stem cell-derived exosomes as a nanotherapeutic agent for amelioration of inflammation-induced astrocyte alterations in mice. Theranostics 2019; 9: 5956-5975.